

# Evolution of magnetic flux in an isolated reconnection process

Gunnar Hornig\*

*Department of Physics and Astronomy,  
Ruhr-Universität Bochum  
44780 Bochum, Germany*

Eric Priest

*School of Mathematics and Statistics,  
University of St. Andrews,  
St. Andrews, KY16 9SS, United Kingdom*

(Dated: February 19, 2003)

A realistic notion of magnetic reconnection is essential to understand the dynamics of magnetic fields in plasmas. Therefore we have modeled a three-dimensional reconnection process in a region of non-vanishing magnetic field and analysed it with respect to the way in which the connection of magnetic flux is changed. The process is localized in space in the sense that the diffusion region is limited to a region of finite radius in an otherwise ideal plasma. We use a kinematic, stationary model which allows for analytical solutions. Aside from the well-known flipping of magnetic flux in the reconnection process, the localization requires additional features which were not present in previous two- and 2.5-dimensional models. In particular, we find rotational plasma flows above and below the diffusion region, which substantially modify the process.

PACS numbers: 52.35.Vd, 95.30.Qd, 52.30.Cv

## I. INTRODUCTION

Magnetic reconnection is a key process of structure formation in space and astrophysical plasmas as well as many technical plasmas. Our previous understanding of the ways magnetic reconnection restructures the magnetic field has been formed largely by the early stationary two-dimensional models where the magnetic field is a planar field with a hyperbolic (X-type) null point [1–4] (see Fig. 1). In these models the magnetic flux is transported towards the null point of the magnetic field by an inflow of plasma, is cut and re-connected at the null point and subsequently the newly connected flux is transported outwards by the plasma flow. The impression of the flux

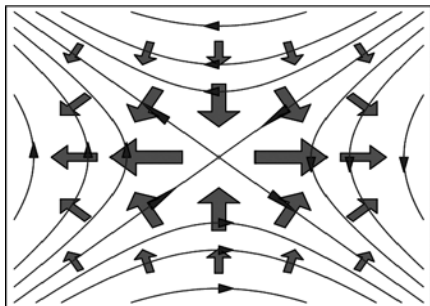


FIG. 1: Sketch of a two-dimensional, stationary reconnection process. The thin lines are magnetic field lines, the thick arrows indicate the transport velocity of magnetic flux.

being cut at the null point can be given a mathematical foundation by defining a transport velocity ( $\mathbf{w}$ ) for the magnetic flux (see e.g. [5]). Given that the process satisfies a resistive Ohm's law

$$\mathbf{E} + \mathbf{v} \times \mathbf{B} = \eta \mathbf{J}, \quad (1)$$

we may define the flux velocity as

$$\mathbf{w} := \mathbf{E} \times \mathbf{B} / |\mathbf{B}^2|, \quad (2)$$

which is possible since in these two-dimensional models  $\mathbf{E}$  is perpendicular to the magnetic field. Thus  $\mathbf{w}$  satisfies

$$\mathbf{E} + \mathbf{w} \times \mathbf{B} = 0 \quad (3)$$

and hence can be considered as transporting the magnetic flux. It can be shown (see [6]) that the singularity of  $\mathbf{w}$  at an X-point of the magnetic field precisely represents a cut and reconnect process for the magnetic flux transported by this flow. If the region in which the non-ideal term ( $\eta \mathbf{J}$ ) is present is limited to a finite region near the null point,  $\mathbf{w}$  will coincide everywhere else with the plasma velocity ( $\mathbf{v}_\perp$ ). In particular the size of the diffusion region does not directly affect the rate at which magnetic flux is reconnected, which is determined solely by the electric field at the null point. This is important for the reconnection in astrophysical plasmas where the extremely small resistivity implies that the non-ideal term becomes relevant only in very localized regions of extreme current concentrations.

Unfortunately, the existence of a flux-transporting velocity ( $\mathbf{w}$ ) with or without singularities is limited to cases where  $\eta \mathbf{J}$ , and therefore  $\mathbf{E}$ , is perpendicular to  $\mathbf{B}$ . Thus, no such velocity exists for cases where  $\mathbf{E} \cdot \mathbf{B} \neq 0$ , which is the case for reconnection in regions of non-vanishing

\*Electronic address: [gh@tp4.ruhr-uni-bochum.de](mailto:gh@tp4.ruhr-uni-bochum.de); URL: <http://www.tp4.ruhr-uni-bochum.de/vw/>

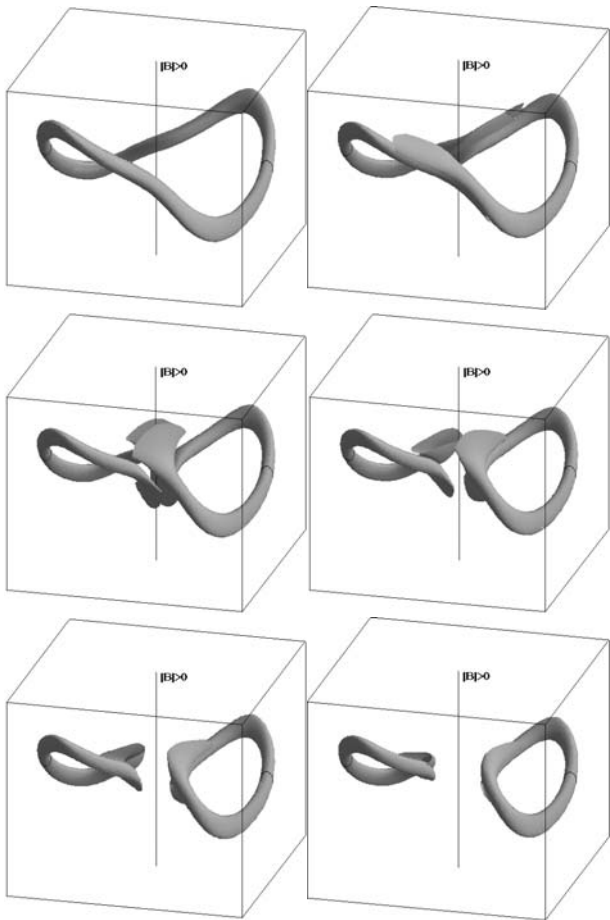


FIG. 2: Splitting and flipping of magnetic flux in the process of reconnection in a region of non-vanishing magnetic field.

magnetic field. See [6, 7] for an explicit proof of this statement. Nevertheless, we can still investigate the evolution of magnetic flux for  $B \neq 0$  reconnection, provided the non-ideal region is limited to a finite region ( $D$ ) which does not contain any closed flux. Under these conditions all the flux in the non-ideal region ( $D$ ) is connected to the ideal environment. Then we can follow the evolution of magnetic flux inside  $D$  by following the magnetic flux frozen to arbitrary cross sections in the ideal external region. There is no flux conserving velocity which satisfies  $\mathbf{w} = \mathbf{v}_\perp$  on the whole boundary of  $D$ , but we can define a flux conserving velocity  $\mathbf{w}$  inside  $D$  which satisfies  $\mathbf{w} = \mathbf{v}$  on either the part of the boundary where flux enters  $D$  or where it leaves  $D$ . We can call them, say,  $\mathbf{w}^{in}$  and  $\mathbf{w}^{out}$ . However, contrary to the two-dimensional case, for the general three-dimensional case  $\mathbf{w}^{in}$  and  $\mathbf{w}^{out}$  will not coincide inside  $D$ . This is the non-existence of a single flux transporting velocity as stated above. The difference of these two velocities results in a splitting of flux tubes entering the non-ideal region as shown in Fig.2 (also see [7]).

Fig.2 also shows the flipping of magnetic flux tubes in the process of reconnection. An important and unsolved

problem is the question about whether or not the corresponding flux tubes join again perfectly when they leave the non-ideal region. Moreover, the process of splitting and flipping of flux tubes has been so far demonstrated for two-dimensional models only (Sometimes called 2.5 dimensional, in which the fields have components in all three directions but they depend on only two coordinates). In these models the diffusion region extends to infinity along the invariant direction. A more realistic model, however, should have a diffusion region which is bounded in all three directions. To investigate this and similar questions we set up a simple analytical magnetohydrodynamic model of reconnection in a domain of non-vanishing magnetic field with a diffusion region localized in three dimensions.

## II. THE MODEL

We seek a kinematic solution of the stationary resistive MHD equations. That is, we want to solve

$$\mathbf{E} + \mathbf{v} \times \mathbf{B} = \eta \mathbf{J}, \quad (4)$$

$$\nabla \times \mathbf{E} = 0, \quad (5)$$

$$\nabla \cdot \mathbf{B} = 0, \quad (6)$$

$$\nabla \times \mathbf{B} = \mu_0 \mathbf{J}, \quad (7)$$

with a localized non-ideal term  $\eta \mathbf{J}$ . The solution for the velocity will turn out to be incompressible ( $\nabla \cdot \mathbf{v} = 0$ ) and therefore allows for a solution of the stationary continuity equation,

$$\nabla \cdot (\rho \mathbf{v}) = 0, \quad (8)$$

for instance with a uniform plasma density ( $\rho = const.$ ).

We start by prescribing the configuration of the magnetic field as a simple superposition of an X-type linear field in the  $x - y$  plane with a homogeneous field in  $z$ -direction,

$$\mathbf{B} = B_0 (y/L \mathbf{e}_x + k^2 x/L \mathbf{e}_y + \mathbf{e}_z). \quad (9)$$

Here  $k$  determines the magnitude of the electric current

$$\mathbf{J} = (k^2 - 1)B_0/(L \mu_0) \mathbf{e}_z. \quad (10)$$

The advantage of this model is that we can integrate the field lines analytically from

$$\frac{\partial \mathbf{X}(s)}{\partial s} = \mathbf{B}(\mathbf{X}(s)) \quad (11)$$

and so obtain the equations  $\mathbf{X}(\mathbf{x}_0, s)$  of the field line that passes through an initial point  $\mathbf{x}_0$ . The components of  $\mathbf{X}(\mathbf{x}_0, s)$  and of the corresponding inverse mapping  $\mathbf{X}_0(\mathbf{x}, s)$  are:

$$X = x_0 \cosh(B_0 k s/L) + y_0/k \sinh(B_0 k s/L) \quad (12a)$$

$$Y = y_0 \cosh(B_0 k s/L) + x_0 k \sinh(B_0 k s/L) \quad (12b)$$

$$Z = z_0 + B_0 s \quad (12c)$$

$$X_0 = x \cosh(B_0 k s/L) - y/k \sinh(B_0 k s/L) \quad (13a)$$

$$Y_0 = y \cosh(B_0 k s/L) - x k \sinh(B_0 k s/L) \quad (13b)$$

$$Z_0 = z - B_0 s. \quad (13c)$$

Note that the parameter  $s$ , which parametrizes the magnetic field line is not the distance  $\lambda$  along the field line, but it is related to it by

$$ds = d\lambda/\|B\|. \quad (14)$$

If we set  $Z_0 = 0$  and solve Eq. 13c for  $s$

$$s = z/B_0, \quad (15)$$

we can replace  $s$  in Eq. 13a and 13b. The corresponding expressions  $X_0(x, y, z)$  and  $Y_0(x, y, z)$  are Euler potentials for the magnetic field, i.e.:

$$\mathbf{B} = \nabla(\sqrt{B_0}X_0) \times \nabla(\sqrt{B_0}Y_0) \quad (16)$$

This property is important for comparison of our results with the theory of ‘General magnetic reconnection’ developed in [8, 9].

Equation 5 implies that the electric field is a gradient of a scalar function  $\phi$ . Inserting this in Eq. 4 yields

$$-\nabla\phi + \mathbf{v} \times \mathbf{B} = \eta \mathbf{J}. \quad (17)$$

In order to have a localized non-ideal term  $\eta \mathbf{J}$  we have to localize the resistivity, since  $\mathbf{J}$  is constant. Note that if we prescribe  $\eta$  we can always calculate  $\phi$  from the component of Eq. 17 parallel to  $\mathbf{B}$ ,  $(\nabla\phi)_{\parallel} = -\eta \mathbf{J}_{\parallel}$ , by integrating along the field lines

$$\phi = - \int \eta \mathbf{J}_{\parallel} dl + \phi_0 = - \int \eta \mathbf{J} \cdot \mathbf{B} ds + \phi_0. \quad (18)$$

To obtain an analytical solution for  $\phi$  we shall prescribe  $\eta$  as the following function of the coordinates  $x_0, y_0$  of field lines in the plane  $z = 0$  and the parameter  $s$  along the field lines.

$$\eta(x_0, y_0, s) = \eta_0 \exp(-(B_0^2 s^2 + x_0^2 + y_0^2)/l^2). \quad (19)$$

Substituting Eq. 13a, 13b and 15 in the expression for  $\eta$  yields  $\eta(x, y, z)$ . This function is positive, has a maximum  $\eta_0$  at the origin and is exponentially decreasing with distance from the origin, such that at a distance of  $2l$  its value is less than 2% of the maximum. We will call this region inside the surface  $\eta = 0.02 \eta_{max}$  the non-ideal region  $D$ . The shape of this domain is a sphere distorted towards a tetrahedron by the hyperbolic structure of the magnetic field (see Fig. 3).

The above method of prescribing the functional form of  $\eta$  is useful for the purpose of identifying the qualitative evolution of magnetic flux, for which only the existence of a non-ideal term and its localization matters rather than its detailed form. The results are to a large extent independent of the profile of the non-idealness. In particular, given a more general Ohm’s law, it does not matter

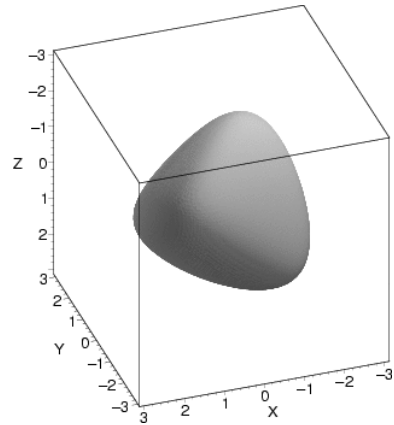


FIG. 3: The non-ideal region  $D$  at 2% of the maximum value of  $\eta$  (parameters:  $k = 2, L = 10, l = 1$ )

whether the non-idealness results from a resistive, inertia or pressure term in Ohm’s law. Important is only the existence of a component parallel to  $\mathbf{B}$ , which is not the gradient of a scalar.

Now we can integrate  $\phi$  from Eq. 18 starting with  $\phi = \phi_0(x_0, y_0)$  in the plane  $z = 0$

$$\phi(x_0, y_0, s) = - \frac{\sqrt{\pi} B_0 \eta_0 l (k^2 - 1) \operatorname{erf}(B_0 s/l)}{2 L \mu_0 \exp((x_0^2 + y_0^2)/l^2)} + \phi_0(x_0, y_0), \quad (20)$$

Again we can use Eq. 13a, 13b and 15 to replace  $(x_0, y_0, s)$  by  $(x, y, z)$  in the expression for  $\phi$ . This allows us to calculate  $\nabla\phi(x, y, z)$  and to deduce the perpendicular component of the plasma velocity:

$$\mathbf{v}_{\perp} = (-\nabla\phi - \eta \mathbf{J}) \times \mathbf{B} / \|\mathbf{B}\|^2. \quad (21)$$

The resulting analytical expression is too long to be presented here explicitly but can be calculated by any computer algebra system immediately. Instead we will use our freedom to add a component parallel to  $\mathbf{B}$  to set the  $z$ -component of the plasma velocity to zero.

$$\mathbf{v} = \mathbf{v}_{\perp} - (\mathbf{v}_{\perp})_z \mathbf{B} / B_0. \quad (22)$$

This is convenient to show plots of the vector field in  $z = \text{const.}$ -planes, without suppressing any information, since now the velocity has only  $x$  and  $y$  components.

The freedom of choosing  $\phi_0(x_0, y_0)$  results from the fact that, for a given magnetic field, Ohm’s law (17) can be decomposed into an ideal and a non-ideal part:

$$-\nabla\phi_{non-id.} + \mathbf{v}_{non-id.} \times \mathbf{B} = \eta \mathbf{J}, \quad (23)$$

$$-\nabla\phi_{id.} + \mathbf{v}_{id.} \times \mathbf{B} = 0. \quad (24)$$

Identifying  $\phi_0$  with  $\phi_{id.}$ , we see that this is the source of an ideal plasma flow which can be superimposed on any reconnection solution. In particular we shall choose

$$\phi_0(x_0, y_0) = \varphi_0 x_0 y_0 / l^2. \quad (25)$$

Again the use of Eq. 13a, 13b and 15 yields the corresponding expression in terms of  $(x, y, z)$ . This choice of  $\phi_0$  corresponds to  $\mathbf{v}_{id.}$  being a stagnation flow. In particular in the  $z = 0$  plane it yields

$$\mathbf{v}_{id.}(z=0) = \phi_0/(B_0 l^2) (-x \mathbf{e}_x + y \mathbf{e}_y). \quad (26)$$

Thus, in the  $z=0$  plane the flow structure of the ideal flow is analogous to the structure of the reconnecting flow shown in Fig. 1. Surprisingly, by comparison with the two-dimensional case,  $\mathbf{v}_{id.}$  is not singular at the origin, since ideal flows can cross the quasi-separatrix surfaces ( $y = \pm kx$ ) when the  $z$ -component of  $\mathbf{B}$  is non-vanishing. It is only when  $\mathbf{B} = 0$  that this results in a singularity in  $\mathbf{v}_{id.}$ .

Before we come to explicit examples two comments may help to clarify the physical nature of the solutions. Firstly, as mentioned above, the velocity is divergence-free, which can be derived from the fact that the  $z$ -component of curl Eq. 17 reduces to  $B_0 \nabla \cdot \mathbf{v} = 0$  due to the constant  $B_z$  and the vanishing  $v_z$ . Therefore the solutions satisfy the continuity equation for a uniform density  $\rho$ .

Secondly, our choice of  $\mathbf{B}$  leads to  $\nabla \times (\mathbf{J} \times \mathbf{B}) = 0$ . Thus we can find a plasma pressure, such that

$$-\nabla P + \mathbf{J} \times \mathbf{B} = 0, \quad (27)$$

i.e., the solutions satisfy the momentum balance in the limit of slow flows (much smaller than the sound and Alfvén speeds). Moreover, we will use in Section IV velocity fields which have a stagnation point in close similarity to the flows which are known to exist for the two-dimensional problem [10, 11] and for which solutions to the full momentum balance exist. Note that the non-vanishing  $B_z$  component does not alter the momentum balance compared to the two-dimensional case, since here  $\mathbf{J}$  has only a  $z$ -component. Thus our kinematic solutions are in a certain limit solutions to the full MHD equations.

### III. PURE SOLUTIONS

We start by analysing the situation when  $\phi_0 \equiv 0$ . For this case the solution for  $\mathbf{v}$  vanishes in the  $z = 0$  plane and shows counter-rotating flows above and below the non-ideal region, as shown in Fig. 4. The rotational flows are distorted by the hyperbolic structure of the magnetic field. Close to the  $z = 0$  plane they are almost circular. For large values of  $z$  they become highly squashed. This effect grows with the ratio  $l/L$ .

Outside the non-ideal domain  $D$ , non-zero flow is limited to regions where  $\phi$  is non-zero. Since  $\phi$  is constant along field lines in the ideal domain, this region consists of all field lines which are threading  $D$ . This domain is itself a flux tube, called a hyperbolic flux tube (see [12] for an exact definition of this term), as shown in Fig. 5.

The existence of rotational flows outside  $D$  (as shown in Fig. 4) can be proved for very general conditions, as

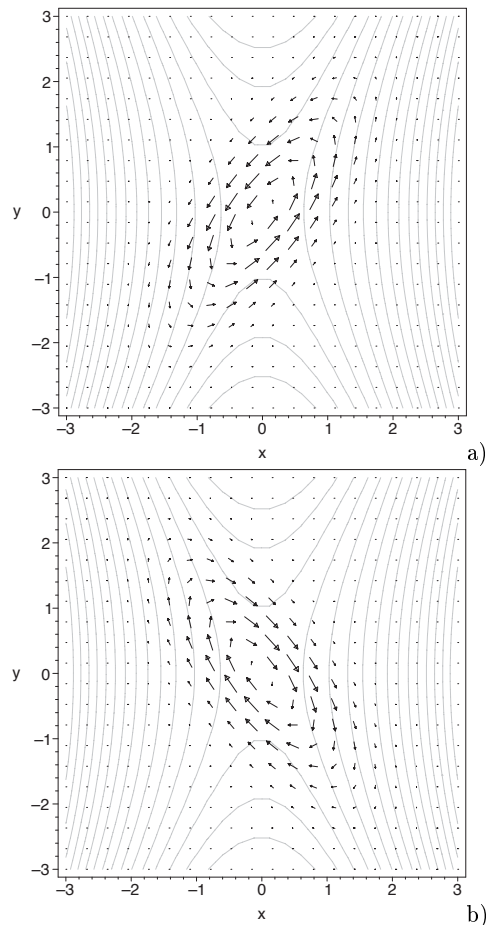


FIG. 4: Counter-rotating plasma flows: a) above ( $z = 2$ ) and b) below ( $z = -2$ ) the reconnection region together with magnetic field lines (grey) for parameters:  $k = 2, L = 10, l = 0$ .

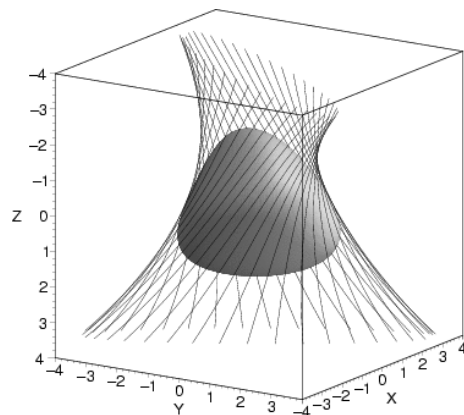


FIG. 5: The non-ideal region  $D$  at 2% of the maximum value of  $\eta$  together with the hyperbolic flux tube enclosing  $D$ , within which the pure solutions have non-vanishing flow (parameters:  $k = 2, L = 10, l = 1$ ).

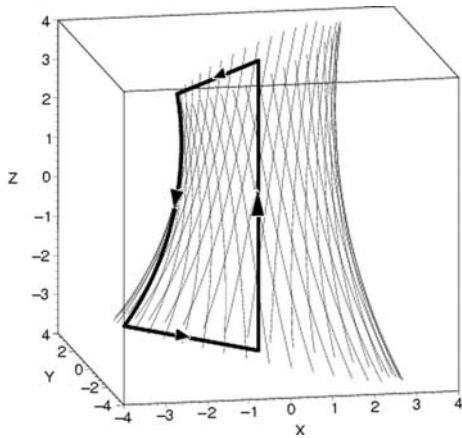


FIG. 6: A closed loop consisting of the central field line and a field line of the envelope together with two radial connections.

follows. Consider the electric field along the central field line,  $x = y = 0$ ,

$$\mathbf{E}(0, 0, z) = B_0 \eta_0 (k^2 - 1) \exp(-z^2/l^2) / (L \mu_0) \mathbf{e}_z. \quad (28)$$

It leads to a potential difference along the central field line above and below  $D$  given by

$$\phi(0, 0, \pm\infty) = \mp \frac{\sqrt{\pi} B_0 \eta_0 l (k^2 - 1)}{2 L \mu_0}. \quad (29)$$

Note that these limiting values are reached to high accuracy already at distances of  $z/l > 2$ . With the same accuracy any field line forming the envelope in Fig. 5 has a vanishing potential  $\phi$  and the same holds for all other field lines outside this hyperbolic flux tube. The central field line ( $L_0$ ), a field line of the envelope ( $L_1$ ) and two radial lines connecting them above and below  $D$  ( $R_1, R_2$ ) form a closed loop ( $L_0, R_1, L_1, R_2$ ). Along this loop the integral over the parallel electric field has to vanish (see Fig. 6), since  $\nabla \times \mathbf{E} = 0$ .

$$\begin{aligned} 0 &= \oint \mathbf{E} \cdot d\mathbf{l} \\ &= \int_{L_0} \mathbf{E} \cdot d\mathbf{l} + \int_{R_1} \mathbf{E} \cdot d\mathbf{l} + \int_{L_1} \mathbf{E} \cdot d\mathbf{l} + \int_{R_2} \mathbf{E} \cdot d\mathbf{l} \\ &= \Delta_{L_0} \phi + \Delta_{R_1} \phi + 0 + \Delta_{R_2} \phi \\ &= 2 \phi(0, 0, -\infty) + 2 \Delta_R \phi. \end{aligned}$$

Here we have used the symmetry  $z \leftrightarrow -z$  in the last equality. Therefore, the voltage drop along each of the radial parts of the loop equals  $-\phi(0, 0, -\infty)$ . However, since the loop integral requires a direction of integration which is opposite for  $R_1$  compared to  $R_2$ , the electric fields along  $R_1$  and  $R_2$  are oppositely directed. These electric fields induce a plasma flow perpendicular to the radial lines in planes of constant  $z$ , which are oppositely directed above and below  $D$ . This completes the proof of the existence of counter-rotating flows.

The existence of rotational flows can be understood from another point of view. In [13] an ideal dynamics

is considered which leads to a current sheet formation in a hyperbolic flux tube. The rotational flows derived above can be considered as the stationary limit of these dynamics if the current density has become sufficiently high that dissipative effects set in and prevent a further increase. In particular, our rotational flows have the same signature as the shearing flows in Fig. 5b of [13].

### A. Reconnected Flux

The rate of reconnected flux is given in general by the integral of the parallel electric field along the reconnection line (see [6, 8]),

$$\frac{d\Phi_{mag.}}{dt} = \int \mathbf{E}_{\parallel} dl. \quad (30)$$

In two-dimensional models the reconnection line is the extension of the hyperbolic null point along the invariant direction. Adding a constant component of  $\mathbf{B}$  in the invariant direction turns the null line into a field line of maximal  $\Delta\phi$  across  $D$ . For our example the rate of reconnected flux is given by  $2\phi(0, 0, -\infty)$ .

The interpretation of a rate of reconnection of magnetic flux in this case, however, is different from what we are used to in two dimensions. In three dimensions no unique line exists at which the flux is split and reconnected: instead, we have a whole flux tube (the hyperbolic flux tube enclosing  $D$ ), within which every field line constantly changes its connection. To envisage the rate of reconnection in this case we will use the method of constructing  $\mathbf{w}^{in}$  and  $\mathbf{w}^{out}$  as described in the introduction. These are the velocities of the field lines in  $D$  anchored in the ideal region either above (outflow region) or below (inflow region)  $D$ . To find these velocities we have to solve

$$-\nabla\phi^{(in/out)} + \mathbf{w}^{(in/out)} \times \mathbf{B} = 0 \quad (31)$$

$$\Rightarrow \mathbf{w}_{\perp}^{(in/out)} = (-\nabla\phi^{(in/out)}) \times \mathbf{B} / \|\mathbf{B}\|^2. \quad (32)$$

Since  $\mathbf{w}^{in}$  and  $\mathbf{w}^{out}$  coincide with  $\mathbf{v}$  outside  $D$  we can use for the corresponding  $\phi^{(in/out)}$  just the asymptotic values of  $\phi$  in Eq. 20 for large  $s$ , i.e., we replace the error function by its asymptotic values 1 and  $-1$

$$\phi_{\frac{in}{out}} = \pm \frac{\sqrt{\pi} B_0 \eta_0 l (k^2 - 1)}{2 L \mu_0 \exp((x_0^2 + y_0^2)/l^2)}. \quad (33)$$

Of course for an explicit calculation we have to replace  $x_0, y_0$  with the help of Eq. 13a, 13b and 15 and insert the result in Eq. 32. If necessary we can also add a flow parallel to  $\mathbf{B}$  to set the  $z$ -component of  $\mathbf{w}$  equal to zero, as we did for  $\mathbf{v}$ .

The rate of ‘mismatching’ of flux is now given by the difference of  $\mathbf{w}^{in}$  and  $\mathbf{w}^{out}$  in  $D$ . For convenience we choose the plane  $z = 0$ , where the relative motion of the two flux tubes anchored in the outflow and inflow region,

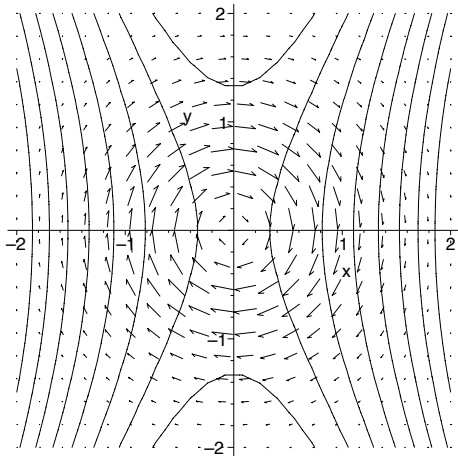


FIG. 7: The difference velocity between flux anchored in the region above and below  $D$  and the projection of magnetic field lines in the plane  $z = 0$  (parameters:  $L = 10, l = 1, k = 2$ )

respectively, is given by:

$$\begin{aligned} \Delta \mathbf{w}_\perp &= -\nabla(\phi^{(out)} - \phi^{(in)}) \times \mathbf{B} / \|\mathbf{B}\|^2 \\ &= -2 \nabla \phi^{out} \times \mathbf{B} / \|\mathbf{B}\|^2. \end{aligned} \quad (34)$$

Fig. 7 shows the corresponding vector field. The rate at which flux crosses any radial line between the origin and the boundary of  $D$  is given by the potential difference along this line, i.e.,

$$\Delta \phi_{\Delta \mathbf{w}} = 2 \phi^{out} = \Delta_{L_0} \phi = 2 \phi(0, 0, -\infty). \quad (35)$$

Note that we now have the same potential difference along a radial line as along the  $z$ -axis ( $L_0$ ), while for the previous integrals along  $R_1$  and  $R_2$  we had only half of this value.

Another important property is the fact that, as in the two-dimensional case, the diameter of the non-ideal region, i.e. its extent in the  $xy$  plane, does not affect the reconnection rate. To prove this we can use different scales, say  $l_{xy}$  and  $l$ , with respect to the  $(x_0, y_0)$ - and  $s$ -dependence in the expression 19 for the resistivity. It then turns out that in  $\phi(0, 0, \pm\infty)$  and hence in the reconnection rate  $l_{xy}$  does not appear. This property is essential for the onset of reconnection under realistic conditions, when the collapse of a current sheet may lead to small scales in the plane perpendicular to the current.

A simple pedagogical example gives further insight into the relation between this potential difference and a reconnection rate. Consider for simplicity a homogeneous magnetic field  $\mathbf{B} = B_0 \mathbf{e}_z$  and assume that the difference velocity is a rigid rotation, with a constant angular velocity  $\omega = 2\pi/T$ . Integrating along a radial line the reconnection rate is then given by

$$\begin{aligned} \frac{d\Phi_{rec}}{dt} &= \int \mathbf{E} \cdot d\mathbf{r} = \int (\mathbf{w} \times \mathbf{B}) \cdot d\mathbf{r} \\ &= 1/T \int 2\pi r B_0 dr = \Phi_{mag}/T. \end{aligned}$$

Thus it takes a full turn for the reconnected flux to be equal to the total magnetic flux of the flux tube  $\Phi_{mag}$ , although already after the first instant all field lines of the flux tube (with exception of the central one) have changed their connections. Note the difference of this notion of reconnection from reconnection rate in the two-dimensional case where the reconnection occurs only at a single line and the reconnection rate gives the amount of flux which is cut by this line.

Up to this point the hyperbolic structure of the magnetic field in the  $xy$ -plane was not relevant for the results, that is for an elliptic field in the  $xy$ -plane (0-point) the results would have been qualitatively the same. The reason is that the existence of counter-rotating flows is a topological property which can be proved without referring to any particular geometry of field lines and even for arbitrary time dependence. This has been done in [14] building on the above mentioned Euler representation of the magnetic field (see also [8, 9]). In particular, the plane for which  $\mathbf{w}^{(in)}, \mathbf{w}^{(out)}$  and  $\Delta \mathbf{w}$  is calculated is arbitrary as long as it is transversal to  $\mathbf{B}$ .

The hyperbolic structure is, however, relevant for the physical background of the reconnection process as discussed above and it will be found to be relevant in Section IV when we consider more realistic reconnection solutions.

## B. The evolution of the magnetic flux

The reconnection process in the foregoing example affects only the hyperbolic flux tube bounding the region  $D$  and even within this flux tube there is a certain order in which the field lines reconnect. To see this note that the level surfaces of  $\phi^{in}$  are also level surfaces of  $\phi^{out}$  (although for different values) and in addition they are flux surfaces for  $\mathbf{B}$  and  $\Delta \mathbf{w}$ , since they satisfy the ideal equation Eq. 31. Thus, the reconnection changes the connection only within each level surface of  $\phi^{(in/out)}$ . There is no reconnection between field lines of different  $\phi^{(in/out)}$  values.

For a given flux tube the process is shown as a sequence of snapshots in Fig. 8. The flux tube first splits into two tubes, which wander in opposite directions along the elliptical flow lines of  $\mathbf{w}^{(in)}$  and  $\mathbf{w}^{(out)}$  shown at the top and bottom of the box. After half a turn they meet again (last frame) and the process repeats itself periodically. What cannot be seen in the sequence of images is that the motion is always very slow near the turning points of the ellipses, whereas it is very fast along the almost straight parts next to the  $z$  axis. If the upper end of a field line is just near a turning point its lower end flips rapidly along the straight part and vice versa. This effect is more pronounced if we follow the field lines further away from the  $z = 0$  plane. The process of flipping is well known from  $2\frac{1}{2}$ -dimensional models ([15]). However, while in the  $2\frac{1}{2}$  dimensional models this is a linear motion extending to infinity, it is here part of a circular motion

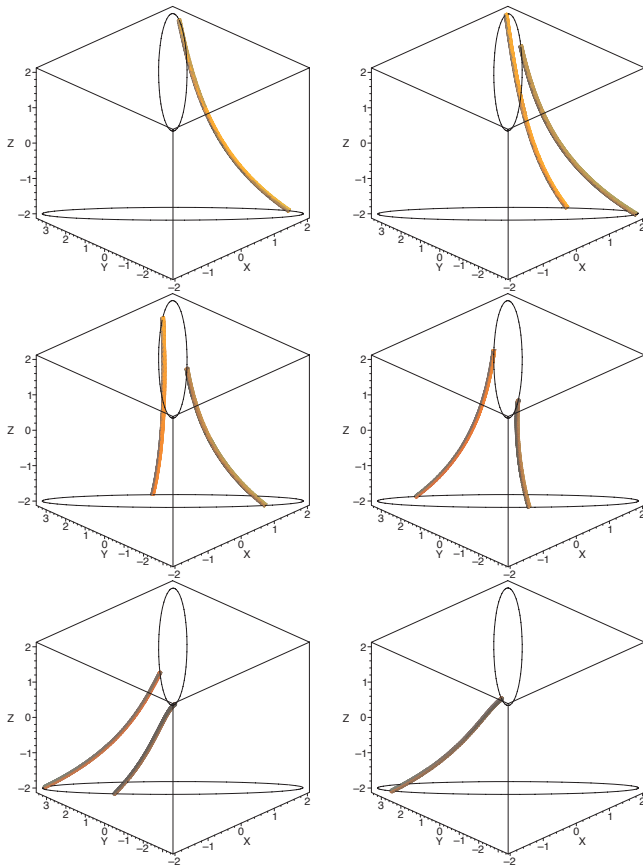


FIG. 8: Splitting of a flux tube under the counter-rotating flows  $\mathbf{w}^{(in)}$  (indicated at the bottom of the box) and  $\mathbf{w}^{(out)}$  (top of the box). After half a turn the two flux tubes meet again (last frame).

due to the finite extension of the non-ideal region.

A remark concerning the production of magnetic helicity in this kind of process: due to  $\mathbf{E} \cdot \mathbf{B}$  being positive (given  $B_0 > 0$  and  $k > 1$ ) we have a non-vanishing source of helicity,  $-2 \int \mathbf{E} \cdot \mathbf{B} dV \neq 0$ . If we imagine that this kind of reconnection takes place in a closed flux tube, which, except for the domain  $D$ , is embedded in an ideal plasma, then due to the counter-rotating flows the process would change the total helicity of the field by twisting or un-twisting the flux tube.

#### IV. COMPOSITE SOLUTIONS

The pure solution can be superimposed on any ideal flow as shown in Eq. 24. Out of all possible ideal flows, however, those with a stagnation flow are of particular interest for two reasons.

First, stagnation flows can create thin current sheets in a self-amplifying way, as shown in several  $2\frac{1}{2}$ -dimensional solutions (see references in [10, 11]). In a real plasma we expect that the main reason for the localization of the non-ideal term is the localization of the current, which

then in turn might trigger a local anomalous resistivity due to turbulent effects on small scales. Thus stagnation flows are often an important prerequisite for having a localized non-ideal term.

Second, the pure solution of the previous section affects only the hyperbolic flux tube enclosing  $D$  and hence is very restricted in its effect on the overall magnetic field. This can be changed if we have a flow which transports flux from the external region into the hyperbolic flux tube, lets it reconnect, and subsequently removes the re-connected flux from this region, thereby extending the effect of the non-ideal region to a much larger domain. Such a process can be accomplished by a stagnation flow.

These are the motivations to use Eq. 25, which creates a stagnation-point flow in the plane  $z = 0$ , as a basic example for the effects of adding an ideal flow to the pure solution. To be more precise, the resulting flow is a stagnation flow outside the hyperbolic flux tube where the pure solution is negligible, but whether the pure solution dominates or not within the hyperbolic flux tube depends on the strength of the ideal flow compared to that of the pure reconnection solution. The parameter which determines the strength of the ideal flow is  $\varphi_0$  in Eq. 25 and the critical value ( $\varphi_{crit}$ ) is the value of  $\varphi_0$  where the flow in  $D$  turns from O-point to X-point.

##### A. Calculation of $\varphi_{crit}$

The critical  $\varphi_0$  at which the nature of the flow changes, may be determined as follows. At  $z = 0$  the rotational flow of the pure solution vanishes. The strength of the rotational flow grows from  $z = 0$  up to the boundary of  $D$ . The local structure of the plasma flow near the  $z$ -axis, which determines whether the flow is X-type or O-type can be deduced from Eq. 21. Note that it is sufficient to use  $\mathbf{v}_\perp$  since  $\mathbf{v} = \mathbf{v}_\perp + \mathcal{O}(x^2)$  and only linear terms are relevant. Near the  $z$ -axis we have

$$\mathbf{v} = -(\nabla\phi)_{xy} \times B_0 \mathbf{e}_z / B_0^2 + \mathcal{O}(x^2), \quad (36)$$

where  $(\nabla\phi)_{xy}$  are the  $x$  and  $y$  components of the gradient. Hence we can decide whether the composite flow is elliptic or hyperbolic by determining whether  $\phi$  has a local extremum or a saddle point in  $x$  and  $y$  on the  $z$ -axis. In addition, the existence of a saddle point or a local extremum in  $\phi$  does not depend on whether we use  $x, y$  or  $x_0, y_0$  coordinates in the plane perpendicular to the  $z$ -axis.

Thus we can make use of  $\phi(x_0, y_0, s)$  from Eq. 20 and expand this in  $x_0, y_0$  at the origin,

$$\begin{aligned} \phi &= a + (b(x_0^2 + y_0^2) + c x_0 y_0) + \mathcal{O}(x^3) \quad \text{with} \\ a &= -\sqrt{\pi} B_0 \eta_0 l (k^2 - 1) / (2L), \\ b &= \sqrt{\pi} B_0 \eta_0 l (k^2 - 1) \operatorname{erf}(z/l) / (2L \mu_0 l^2), \\ c &= \varphi_0 / l^2. \end{aligned}$$

The critical value which distinguishes whether  $\phi$  has a local extremum or a saddle point is  $c^2 - 4b^2$  or in other

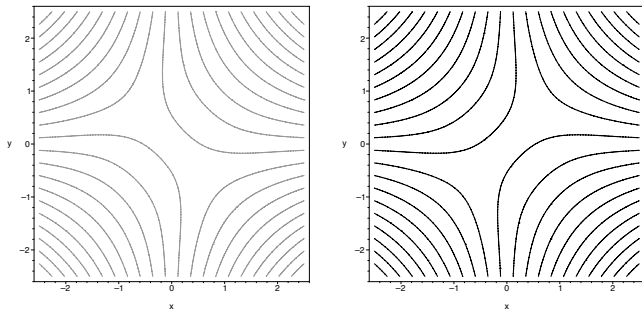


FIG. 9: The flow lines of  $\mathbf{w}^{in}$  (left) and  $\mathbf{w}^{out}$  (right) in the  $z = 0$  plane for parameters  $k = 2$ ,  $\eta_0 = 0.001$ ,  $L = 2$ ,  $l = 1$ ,  $B_0 = 3$ ,  $\varphi_0 = 0.01 > \varphi_{crit.}$ .

words the critical value of  $\varphi_0$  is

$$\varphi_{crit}^2(z) = \pi B_0^2 \eta_0^2 l^2 (k^2 - 1)^2 \text{erf}^2(z/l) / (L^2 \mu_0^2). \quad (37)$$

Since the error function is bounded by  $\pm 1$  there is a maximum of this value:

$$\varphi_{crit} = \sqrt{\pi} B_0 \eta_0 l |k^2 - 1| / (L \mu_0). \quad (38)$$

The same critical value holds for  $\mathbf{w}^{in}$  and  $\mathbf{w}^{out}$  since they are derived from  $\phi$  by replacing the error function by  $\pm 1$  right from the start. Thus, for  $\varphi_0 > \varphi_{crit.}$   $\mathbf{w}^{in}$ ,  $\mathbf{w}^{out}$  and  $\mathbf{v}$  have a stagnation point at  $x = y = 0$  for every  $z$ . For  $\varphi_0 < \varphi_{crit.}$   $\mathbf{w}^{in}$  and  $\mathbf{w}^{out}$  show an elliptic flow at  $x = y = 0$  for every  $z$ . The same is true for  $\mathbf{v}$  outside  $D$ . Inside  $D$  there is a critical distance from  $z = 0$  at which we have a transition from a hyperbolic to an elliptic point in  $\mathbf{v}$ .

## B. Evolution of the magnetic flux

The effect of the additional flow on the reconnection process can be visualized best by the flows  $\mathbf{w}^{in}$  and  $\mathbf{w}^{out}$  in the  $z = 0$  plane, or even simpler by plotting contour levels of  $\phi^{(in)}$  and  $\phi^{(out)}$  at  $z = 0$ , which coincide with flow lines  $\mathbf{w}^{in}$  and  $\mathbf{w}^{out}$ , respectively. In Fig. 9 we show these lines for a case where  $\varphi_0 > \varphi_{crit.}$ , that is, we have stagnation flows in both  $\mathbf{w}^{in}$  and  $\mathbf{w}^{out}$ .

The effect of reconnection on the magnetic flux can now be demonstrated by superimposing the two flow-line images, such that the deviations from ideal flow become apparent. This is shown in Fig. 10, which may be read in the following way. Any point in the diagram represents a given field line. Starting with a given point (field line) there are always two flow-lines of  $\mathbf{w}^{in}$  and  $\mathbf{w}^{out}$  intersecting at this point. They trace the path of the initial point (field line) frozen to  $\mathbf{w}^{in}$  (left) and  $\mathbf{w}^{out}$ , respectively. Whenever the flow-lines cross at a given point a field line starting in this field will split into two if we follow both motions.

There are three types of matching or mismatching of magnetic field lines related to three types of regions in

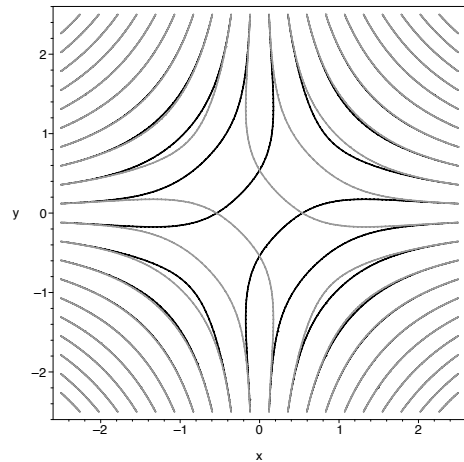


FIG. 10: The superposition of the two flows in Fig. 9 shows regions of different reconnective behaviour, depending on whether the flow lines of  $\mathbf{w}^{in}$  and  $\mathbf{w}^{out}$  coincide or separate.

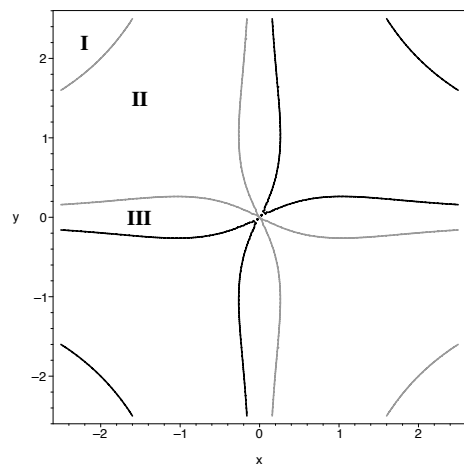


FIG. 11: The separatrices of  $\mathbf{w}^{in}$  and  $\mathbf{w}^{out}$  from Fig. 10 distinguish the regions which show almost classical reconnection (III), from the ideal region (I) together with the transition region (II).

this diagram, as shown in Fig. 11. First, for all flow lines which remain outside  $D$  (which is limited by  $r \sim 2$  and indicated as type I in Fig. 11) the two flow lines coincide perfectly. Moreover, the values of  $\mathbf{w}^{in}$  (left) and  $\mathbf{w}^{out}$  coincide, so that any field line of  $\mathbf{B}$  threading the  $z = 0$  plane at such flow lines is frozen-in ( $\mathbf{w}^{in} = \mathbf{w}^{out} = \mathbf{v}$ ).

Second, there are cases where the flow lines of  $\mathbf{w}^{in}$  and  $\mathbf{w}^{out}$  separate only for a small part inside  $D$  and join again as they leave  $D$  (region of type II in Fig. 11). A magnetic field line transported by this flow towards  $D$  will show a splitting into two of a field line entering  $D$ , and this splitting can remain even after both field lines have left  $D$ , since it might take both field lines different times to leave  $D$ . However, since the flow lines join again, the separation in time of the split field lines remains constant once they have left  $D$ .

Third, there are cases where the flow lines separate

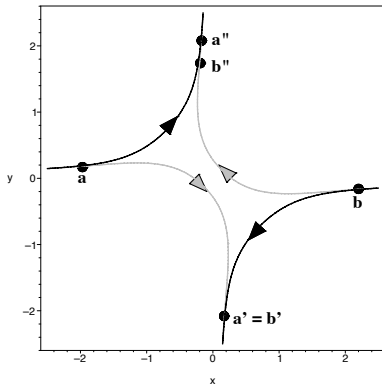


FIG. 12: The transport of fluid elements in the reconnecting flows of region III. Two starting points  $a$  and  $b$  were chosen such that they join at  $a' = b'$  but they will in general not match on the other side.

within  $D$  and join with flow lines of opposite regions leaving  $D$  (regions of type III). A magnetic field line transported by this flow towards  $D$  will show a splitting in  $D$ , and will merge with field lines of a different region on leaving  $D$ . In particular, the distance in space or time of its initial partner grows even after both have left  $D$ . This distinguishes them from the previous case. The region of initial points which show this behaviour is bounded by the separatrices of the two flows shown in Fig. 11. This case is very similar to the ‘classical’ two-dimensional reconnection in that field lines of very distant regions become newly connected.

However, there is in general no unique counterpart to a given field line. This is demonstrated in Fig. 12 for a single set of flow lines from region III. Starting with a fluid element ( $a$ ) at an initial time we can find a counterpart ( $b$ ) such that they coincide once they have left  $D$  in the negative  $y$ -direction ( $a' = b'$ ) but they will in general not match at the opposite side, i.e.  $a'' \neq b''$ . (For symmetry reasons the  $x$  axis in our example is exceptional in that here we can find perfect counterparts). A field line, let us call it ( $a'''$ ), which joins with ( $b''$ ) lies on the same flow line as ( $a$ ) but is shifted by a certain interval in time. If we iterate the process of finding the reconnecting counterparts, i.e. using ( $a'''$ ) as a new ( $a$ ) and so on, we always obtain points which lie on the four trajectories shown in Fig. 12. So the counterparts of this reconnection process are not two field lines but the two flux surfaces given by the field lines crossing the inflow trajectories.

This implies that in general any flux tube will not have a counterpart with which it can reconnect perfectly in this stationary example. Note that by this process we always remain on the same level of  $\phi^{(in)}$  or  $\phi^{(out)}$  since we switch between  $\phi^{(in)}$  and  $\phi^{(out)}$  only outside  $D$  where they coincide. The regions of type III for which the field lines show genuine reconnection grow with  $\eta_0$  until  $\varphi_0$  reaches the critical value.

Further increase of  $\eta_0$  changes the flow pattern drasti-

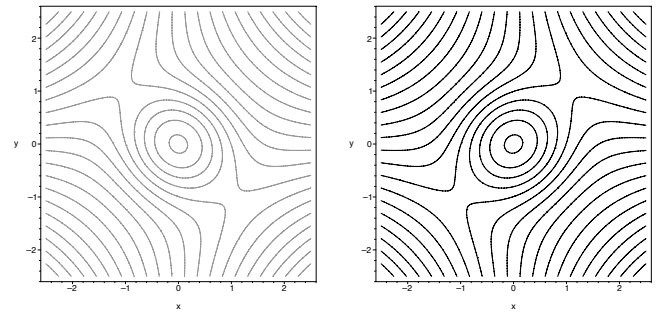


FIG. 13: The flow lines of  $w^{in}$  (left) and  $w^{out}$  (right) in the  $z = 0$  plane for parameters  $k = 2$ ,  $\eta_0 = 0.01$ ,  $L = 2$ ,  $l = 1$ ,  $B_0 = 3$  and  $\varphi_0 = 0.01 < \varphi_{crit.}$ .

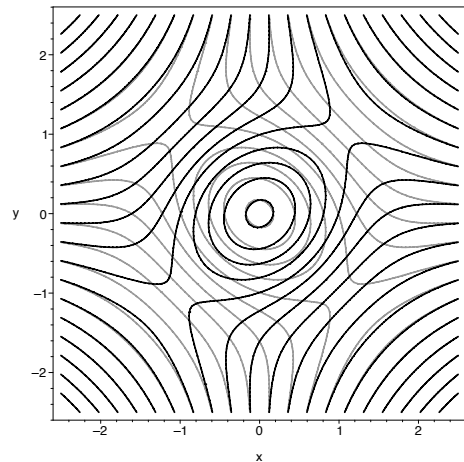


FIG. 14: The superposition of the two flows for  $\varphi_0 < \varphi_{crit.}$  (from Fig. 13) shows regions of different reconnective behaviour.

cally. This is shown in Fig. 13 for the two flows separately and in Fig. 14 for the superposition. Fig. 15 shows the different types of region. Apart from regions I-III which are known from the previous example, there are now two new regions IV and V which result from the existence of the elliptic null in the center. Note that both regions are strictly within the hyperbolic flux tube and have no effect on the reconnective behaviour of the hyperbolic flux tube with its environment. Only the size of the regions I-III are important for the interaction with the environment. The region V in particular shows a dynamics similar to the pure reconnection solution. An initial field line splits under the influence of counter-rotating flows, but both parts rejoin after some time. Here the counter-rotating flows are dominant. Region IV is a kind of transition region between III and V. Here an initial field line splits, one part remains within the hyperbolic flux tube while the other leaves this domain.

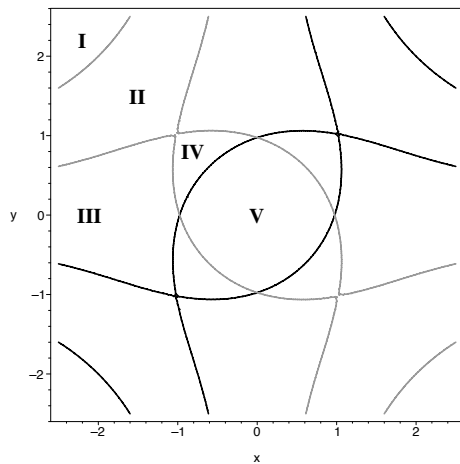


FIG. 15: The separatrix structure of Fig. 14. Regions of type I-III are the same as in the previous example. Regions of type IV and V result from the existence of an elliptic null point in the flows for  $\varphi < \varphi_{crit.}$ .

### C. Reconnection rate

The consideration concerning the reconnected flux in Section III A still holds for the composite solution. In particular we can construct the flows  $\mathbf{w}^{in}$  and  $\mathbf{w}^{out}$  and their difference  $\Delta\mathbf{w}$ . Note that while  $\mathbf{w}^{in}$  and  $\mathbf{w}^{out}$  depend on the ideal flow induced by  $\phi_0$ ,  $\Delta\mathbf{w}$  does not and hence it is just the same as for the pure solution and so is the interpretation of  $\Delta\mathbf{w}$  as the reconnecting engine. However, for the composite solutions the reconnection rate summarizes the effect of two ( $\varphi_0 > \varphi_{crit.}$ ) or four ( $\varphi_0 < \varphi_{crit.}$ ) quite different kinds of reconnective behaviour. The almost classical type of reconnection of region III, the more slippage like behaviour of region II and additionally the rotational reconnection of region V together with transitional form of region IV for ( $\varphi_0 < \varphi_{crit.}$ ).

Note that the superposition of the ideal stagnation flow, although non-reconnective in itself, plays an important role in the process. It transports flux to  $D$ , where the reconnection occurs, and subsequently removes the reconnected flux. It is only due to the stagnation flow that a separation of the reconnected flux over larger distances occurs, as has been mentioned already in [8].

## V. TIME DEPENDENCE

The model can be easily modified to include time dependence. For instance we can multiply the first term in Eq. 20 by a time-dependent factor. In addition, also the second term may contain a time-dependence, as follows

$$\phi(x_0, y_0, s) = -f(t) \frac{\sqrt{\pi} B_0 \eta_0 l (k^2 - 1) \operatorname{erf}(B_0 s/l)}{2 L \mu_0 \exp((x_0^2 + y_0^2)/l^2)} + \phi_0(x_0, y_0, t), \quad (39)$$

Since the electric field is still a gradient of a scalar function, no additional magnetic field is induced and the time-dependence shows up only in  $\phi$  and  $\mathbf{v}$  or  $\mathbf{w}^{in/out}$ .

From the variety of solutions generated in this way we will consider here only one which yields a reconnection process localized in time, that is, we suppose

$$f(t) = \exp(-t^2/T^2), \quad (40)$$

and adopt the same steady  $\phi_0(x_0, y_0)$  as before. For most aspects discussed in the previous section the time-dependence is not important since it is in many respects like an external parameter. However, as far as the existence of flux tubes which join perfectly after reconnection is concerned the time-dependence is important. To find such flux tubes we start with a point in the inflow region near the  $x$ -axis and integrate for a given time  $\tilde{t}$  along  $\mathbf{w}^{(in)}$  until we have crossed  $D$ . Then we integrate backwards in time for the same period along  $\mathbf{w}^{(out)}$ : that is, we follow the field lines in Fig. 12 from point  $(a)$  over  $(b')$  to  $(b)$ . We integrate further forward along  $\mathbf{w}^{(in)}$  to  $(b'')$  and then again backward in time along  $\mathbf{w}^{(out)}$ .

For a starting point on the  $x$  axis the full loop would bring us back to the starting point. For other points in  $D$  we will in general end at a different point  $(a'')$ . If  $(a)$  belongs to the cross section of a flux tube which has a counterpart such that they join perfectly in the process of reconnection, then  $(a'')$  has to be a point of this cross section as well. Thus iterating this procedure for a large number  $N$  should trace out the cross section of such a flux tube, if it exists. For a reconnection process localized in time such a procedure shows perfectly-reconnecting cross-sections in a very narrow region near the  $x$ -axis. The results are shown in Fig. 16 for various degrees of localization in time, given by the value of  $T$ . The plots show the points  $a, a''', \dots$  near the negative  $x$ -axis and on the other side their counterparts. The figure shows that with increasing  $T$ , that is, if the process becomes more and more stationary, the cross section stretches. For  $T = 1000$ , which from the numerical point of view is equivalent to the stationary process, the points remain always on the same field line of  $\mathbf{w}^{(out)}$  or  $\mathbf{w}^{(in)}$ , respectively. This confirms the considerations from above that for this case the points will remain on the same level curve of  $\phi^{(in)}$  or  $\phi^{(out)}$ , respectively.

The existence of perfectly reconnecting cross-sections is consistent with the production of magnetic helicity, as mentioned in Section III B. For such a cross section the final flux tubes shows a rotation in the connection of field lines with respect to the state before the reconnection, similar to the pure reconnection case. However, while in the stationary pure reconnection case the rotation increases in time, the localization in time leads here to a rotation by a finite angle. This rotation also shows that there cannot be a one-to-one reconnection of field lines and it is a manifestation of the helicity production in the process.

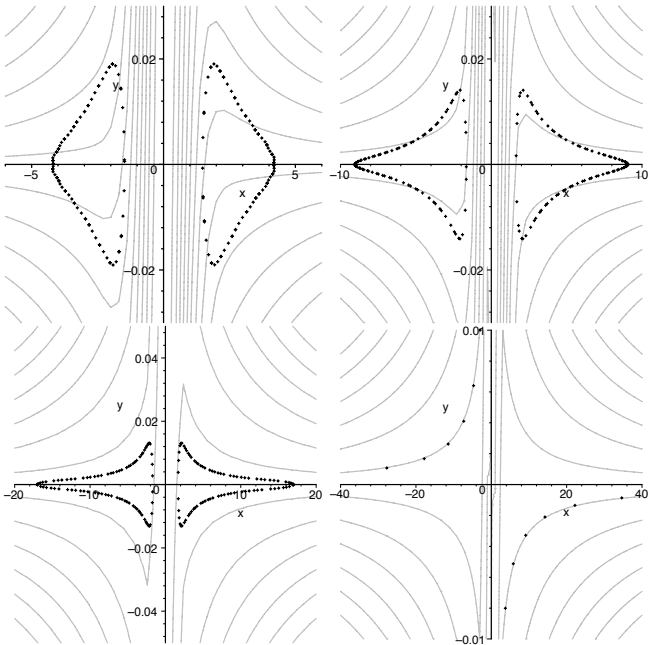


FIG. 16: Perfectly reconnecting cross section for reconnection localized in time on time scales  $T = 30$ ,  $T = 60$ ,  $T = 100$  and  $T = 1000$  for parameters  $k = 2$ ,  $\eta_0 = 0.1$ ,  $L = 2$ ,  $l = 1$ ,  $B_0 = 2$ ,  $\varphi_0 = 1 > \varphi_{crit.}$ .

## VI. CONCLUSIONS

The process of three-dimensional magnetic reconnection at a localized non-ideal region of a non-vanishing

magnetic field shows features which have been not present in previous two- (or 2.5-) dimensional models. The localisation implies the existence of rotational flows above and below the non-ideal region (with respect to the direction of the magnetic field). Moreover, stationary reconnection is imperfect for most of the field lines in the sense, that there is no ‘cross-connection between pairs of field lines, i.e. the strict one to one correspondence of reconnecting field lines known from two-dimensional reconnection is broken in the three-dimensional case. It has to be replaced by a weaker form of a reconnection of field lines from two flux surfaces. For a reconnection localized in time some of these flux surfaces close to form perfectly reconnecting flux-tubes. These tubes show that in the three-dimensional process, although much more complicated than the two-dimensional case, there is still a systematic order in which the flux is reconnected.

## Acknowledgments

G.H. wishes to thank the Solar Physics Group in St. Andrews for their hospitality and acknowledges financial support by the VW-Foundation. Both authors wish to thank K. Schindler for helpful comments and acknowledge support by the European Community’s Human Potential Program under contract HPRN-CT-2000-00153, PLATON.

- 
- [1] P. Sweet, *Nuovo Cimento Ser. X* **8**, 188 (1958).
  - [2] E. Parker, *J. Geophys. Res.* **62**, 509 (1957).
  - [3] H. Petschek, in *Physics of Solar Flares*, edited by W. Hess (NASA SP50, Washington DC, 1964), pp. 425–439.
  - [4] E. Priest and T. Forbes, *J. Geophys. Res.* **91**, 5579 (1986).
  - [5] G. Hornig and K. Schindler, *Physics of Plasmas* **3**, 781 (1996).
  - [6] G. Hornig, in *An Introduction to the Geometry and Topology of Fluid Flows*, edited by R. Ricca (Kluwer, 2001), pp. 295–313.
  - [7] E. Priest, G. Hornig, and D. Pontin, *J. Geophysical Research* **xx**, xx (2003), submitted.
  - [8] K. Schindler, M. Hesse, and J. Birn, *J. Geophysical Research* **93**, 5547 (1988).
  - [9] M. Hesse and K. Schindler, *J. Geophysical Research* **93**, 5559 (1988).
  - [10] E. Priest and T. Forbes, *Magnetic Reconnection* (Camb. Univ. Press, 2000).
  - [11] D. Biskamp, *Magnetic Reconnection* (Camb. Univ. Press, 2000).
  - [12] V. Titov, G. Hornig, and P. Demoulin, *J. Geophys. Res.* **107(A8)**, 1164, doi:10.1029/2001JA000278 (2002).
  - [13] V. Titov, K. Galsgaard, and T. Neukirch, *Astrophys. J.* **582 (2)**, accepted (2003).
  - [14] K. Schindler, in *Physics of the Magnetopause* (AGU, 1995), p. 197.
  - [15] E. Priest and T. Forbes, *J. Geophys. Res.* **97**, 1521 (1992).

Produces the bibliography via BibTeX.